CALL FOR PAPERS | *Neurophysiology of Tactile Perception: A Tribute to Steven Hsiao*

Normalization in human somatosensory cortex

Gijs Joost Brouwer,[1] Vanessa Arnedo,[2] Shani Offen,[1] David J. Heeger,[1] and Arthur C. Grant[2]

[1]*Department of Psychology and Center for Neural Science, New York University, New York, New York; and* [2]*Department of Neurology, State University of New York, Downstate Medical Center, Brooklyn, New York*

Brouwer GJ, Arnedo V, Offen S, Heeger DJ, Grant AC. Normalization in human somatosensory cortex. *J Neurophysiol* 114: 2588–2599, 2015. First published August 26, 2015; doi:10.1152/jn.00939.2014.— Functional magnetic resonance imaging (fMRI) was used to measure activity in human somatosensory cortex and to test for cross-digit suppression. Subjects received stimulation (vibration of varying amplitudes) to the right thumb (target) with or without concurrent stimulation of the right middle finger (mask). Subjects were less sensitive to target stimulation (psychophysical detection thresholds were higher) when target and mask digits were stimulated concurrently compared with when the target was stimulated in isolation. fMRI voxels in a region of the left postcentral gyrus each responded when either digit was stimulated. A regression model (called a forward model) was used to separate the fMRI measurements from these voxels into two hypothetical channels, each of which responded selectively to only one of the two digits. For the channel tuned to the target digit, responses in the left postcentral gyrus increased with target stimulus amplitude but were suppressed by concurrent stimulation to the mask digit, evident as a shift in the gain of the response functions. For the channel tuned to the mask digit, a constant baseline response was evoked for all target amplitudes when the mask was absent and responses decreased with increasing target amplitude when the mask was concurrently presented. A computational model based on divisive normalization provided a good fit to the measurements for both mask-absent and target + mask stimulation. We conclude that the normalization model can explain cross-digit suppression in human somatosensory cortex, supporting the hypothesis that normalization is a canonical neural computation.

fMRI; somatosensory cortex; suppression; normalization; forward model

SOMATOSENSORY STIMULATIONS delivered concurrently at two nearby locations on the skin may interfere with one another to reduce their detectability (masking), a phenomenon that has been attributed to mutual suppression between neurons that respond selectively to each of the two stimuli (Gardner and Spencer 1972a, 1972b; Tommerdahl et al. 2010). Such suppressive effects have been reported in human somatosensory cortex with EEG (Gandevia et al. 1983), MEG (Hoechstetter et al. 2001), and functional magnetic resonance imaging (fMRI) (Krause et al. 2001; Kurth et al. 2000; Ruben et al. 2006). For example, concurrent stimulation of the fingertips evokes less activity than sequential stimulation of the same fingertips

(Gandevia et al. 1983; Hoechstetter et al. 2001). Analogous suppressive effects have been reported in the visual system, and they have been attributed to a particular computational theory of neural processing called the normalization model. Normalization in the visual system provides a variety of useful functions including maximizing sensitivity for some stimulus features while maintaining invariance with respect to other stimulus dimensions and improving the efficiency of sensory coding (Carandini et al. 1997). The same principles of maximizing sensitivity, maintaining invariance, and optimizing efficiency apply also to somatosensory coding in somatosensory systems. Do neural circuits in the primary somatosensory cortex (S1) perform the same computation, i.e., normalization, that is performed by the visual system and other sensory systems?

The normalization model was initially proposed to explain stimulus-evoked responses of individual neurons in primary visual cortex (V1) (Carandini et al. 1997; Carandini and Heeger 1994; Heeger 1992). The model's defining characteristic is that the response of each neuron is divided by a factor that includes the summed activity of a pool of neurons (Carandini and Heeger 2012). In V1, this normalization pool includes neurons selective for a range of different visual stimulus features (e.g., orientation, spatial frequency, motion direction, binocular disparity, eye dominance) and spatial positions (i.e., receptive field locations). The model thereby predicts and explains well-documented physiological phenomena, such as cross-orientation suppression, in which a V1 neuron's response to its preferred orientation is suppressed by simultaneous presentation of the orthogonal orientation (which does not evoke any response when presented alone), and surround suppression, in which a neuron's response to a preferred stimulus within its receptive field is suppressed by simultaneous stimulation at nearby positions outside the receptive field (Carandini et al. 1997; Cavanaugh et al. 2002a, 2002b; DeAngelis et al. 1992; Geisler and Albrecht 1992; Morrone et al. 1982; Morrone and Burr 1986; Sceniak et al. 1999, 2001; Smith et al. 2006). Similarly, the normalization model accurately fits the pooled activity of large populations of neurons in cat V1 (Busse et al. 2009), visual-evoked potentials in human subjects (Busse et al. 2009), and fMRI measurements of activity in human V1 (Brouwer and Heeger 2011; Moradi and Heeger 2009; Zenger-Landolt and Heeger 2003). The model likewise fits psychophysical measurements of pattern masking

Address for reprint requests and other correspondence: D. J. Heeger, Dept. of Psychology and Center for Neural Science, New York Univ., New York, NY 10003 (e-mail: david.heeger@nyu.edu).

and surround masking (Foley 1994; Xing and Heeger 2000, 2001), which are the hypothesized perceptual analogs of cross-orientation suppression and surround suppression. The model has since been shown to explain stimulus-evoked responses in visual cortical area MT (Simoncelli and Heeger 1998), infero-temporal cortex (Zoccolan et al. 2005), and primary auditory cortex (e.g., Rabinowitz et al. 2011), multisensory integration in MST (Ohshiro et al. 2011), the representation of value in LIP (Louie and Glimcher 2010), responses of neurons in the superior colliculus and their role in the control of saccadic eye movements (Vokoun et al. 2014), olfactory processing in *Drosophila* antennal lobe (Olsen et al. 2010), and modulatory effects of attention on visual cortical neurons (Herrmann et al. 2010; Itthipuripat et al. 2014; Reynolds and Heeger 2009; Sundberg et al. 2009). It has been hypothesized, consequently, that the brain relies on a set of canonical neural computations, repeating them across brain regions and modalities to apply similar operations of the same form, hierarchically, giving rise to greater selectivity and invariance at each stage of visual processing (Heeger et al. 1996; Riesenhuber and Poggio 1999, 2002; Simoncelli and Heeger 1998), and that divisive normalization may be one of these canonical neural computations (Carandini and Heeger 2012).

In both humans and nonhuman primates, S1, located on the postcentral gyrus, contains a somatotopic map of the body. This map can be divided further, based on differences in physiology and cytoarchitecture, into four distinct subregions (3a, 3b, 1, and 2), each containing a complete representation of the hand and digits (Geyer et al. 1997, 1999, 2000; Sanchez-Panchuelo et al. 2012). In nonhuman primates, these subregions differ in the average size of the receptive fields: area 3b receptive fields are restricted to a single digit (Iwamura et al. 1983a; Pons et al. 1987), but receptive field sizes are larger in areas 1 and 2, extending over multiple digits (Hyvarinen and Poranen 1978; Iwamura et al. 1983a, 1983b). There is an analogous complex pattern of overlapping cortical representations for different fingertips within human S1 (Besle et al. 2013). With high-resolution fMRI (7 T, 1.25 × 1.25 × 1.3-mm voxels), distinct representations of the fingertips are evident only in the anterior part of S1 (mainly in the posterior bank of the central sulcus, although for some subjects it extends onto the postcentral gyrus), whereas voxels in the posterior part of S1 (on the postcentral gyrus) generally respond to more than two fingertips (Besle et al. 2013, 2014). There is some overlap between the fMRI responses to adjacent fingertips even in the anterior part of S1, with many voxels responding to two adjacent fingertips, but there is more overlap in the posterior part of S1, with many voxels responding to five fingertips (Besle et al. 2014). The overlap is not entirely due to the spatial spread of the hemodynamic responses (Besle et al. 2014), consistent with the observations (cited above) that receptive fields extend over multiple digits in nonhuman primates. This overlap in the cortical representation of different fingertips makes it difficult to quantify the suppression induced by stimulating one digit on the responses evoked by concurrent stimulation of a second digit.

A regression model (called a forward model) can be used to separate the responses of distinct subpopulations of neurons that are intermingled at a fine spatial scale, e.g., subpopulations of neurons in V1 with different orientation preferences (Brouwer and Heeger 2011; Kay et al. 2008). With a forward model, voxel responses are transformed into a small number of idealized channel responses, where the channels are selective for stimulus features. We have used this approach successfully to characterize the representation of color (Brouwer and Heeger 2009, 2013) and, more relevant to the present study, cross-orientation suppression (Brouwer and Heeger 2011). In cross-orientation suppression, the response to a grating at the neuron's preferred orientation (target) is suppressed by the simultaneous presentation of an orthogonal (mask) grating (Carandini et al. 1997; DeAngelis et al. 1992; Geisler and Albrecht 1992; Morrone et al. 1982). We previously reported using fMRI to measure cortical activity as a function of contrast for (vertically oriented) target gratings and for "plaids" in which (vertically oriented) target gratings were superimposed with a (horizontally oriented) mask grating, and we used a forward model to transform the voxel responses into a small set of orientation-selective channels (Brouwer and Heeger 2011). The normalization model provided a good fit to the channel responses. For the channel tuned to the target orientation (vertical), responses increased with target contrast but were suppressed when the horizontal mask was added, evident as a shift in the contrast gain of this channel's responses. For the channel tuned to the mask orientation (horizontal), a constant baseline response was evoked for all target contrasts when the mask was absent and responses decreased with target contrast when the mask was present.

In the present study, we used a very similar methodology to characterize cross-digit suppression in human somatosensory cortex. We found that the activity produced by stimulating one digit (thumb) was suppressed by a concurrent stimulation of a different digit (middle finger). Furthermore, the suppression was evident as a shift in gain, as explained by the normalization model. This result supports the hypothesis that normalization is a canonical neural computation that is implemented in many different neural systems.

MATERIALS AND METHODS

Subjects and scanning sessions. Six healthy subjects between the ages of 21 and 35 yr participated in the fMRI experiment, and a separate group of five subjects participated in the psychophysics experiment. Subjects provided written informed consent. Experimental procedures were in compliance with the safety guidelines for MRI research and were approved by the University Committee on Activities Involving Human Subjects at New York University. Subjects had normal or corrected-to-normal vision and no history of somatosensory dysfunction, peripheral neuropathy, or finger calluses. Each fMRI subject participated in two experimental sessions of the main experiment, consisting of 10 runs each. Subjects also participated in a session in which three high-resolution anatomical volumes were acquired.

Tactile and visual stimulus presentation. Tactile stimuli were delivered to the distal pad of the subjects' right thumb and middle finger with two independent, custom-built, MR-compatible piezoelectric devices (PTS-C2 piezo tactile stimulator; Dancer Design). Each stimulator delivered a somatosensory stimulus at a frequency of 25 Hz with ~1-mm displacement applied over an ~1-mm^2 area of contact. Visual stimuli were presented with an LCD projector (Eiki LC-XG100; Eiki, Rancho Santa Margarita, CA) with a pixel resolution of 1,024 × 768 and a 60-Hz refresh rate. Subjects viewed the image from the LCD projector on a rear projection screen placed inside the bore of the magnet at a distance of 57 cm, yielding a field of view of 32° × 20°.

MRI acquisition. MRI data were acquired with a 3-T, head-only MRI scanner (Allegra; Siemens, Erlangen, Germany) using a head coil (NM-011; NOVA Medical, Wakefield, MA) for transmitting and an eight-channel phased array surface coil (NMSC-071; NOVA Medical) for receiving. Functional scans were acquired with gradient recalled echo-planar imaging to measure blood oxygen level-dependent (BOLD) changes in image intensity (Ogawa et al. 1990). Functional imaging was conducted with 24 slices oriented parallel to the AC/PC plane and positioned over the pre- and postcentral gyri, containing the primary motor cortex and S1, respectively (repetition time: 1.5 s; echo time: 30 ms; flip angle: 75°; voxel size: $2 \times 2 \times 2.5$ mm; 64×64 grid size). A T1-weighted magnetization-prepared rapid gradient echo (MPRAGE, $1 \times 1 \times 2.5$ mm) anatomical volume was acquired in each scanning session with the same slice prescriptions as the functional images. This anatomical volume was aligned with a robust image registration algorithm (Nestares and Heeger 2000) to a high-resolution anatomical volume. The high-resolution anatomical volume, acquired in a separate session, was the average of several MPRAGE scans ($1 \times 1 \times 1$ mm) that were aligned and averaged and was used not only for registration across scanning sessions but also for gray matter segmentation and cortical flattening (see below).

Stimuli and experimental protocol. Tactile stimuli consisted of 1.5-s bursts of sinusoidally modulated displacement of the piezoelectric element at 25 Hz, which was experienced as "flutter." A target stimulus was presented to the thumb at five different amplitude levels (1.56%, 3.125%, 6.25%, 12.5%, and 50% of maximum vibration level) either in isolation ("mask absent") or concurrent with a mask stimulus presented to the middle finger at 50% of maximum vibration level ("target + mask"). In addition, we included separate "mask-only" and "target-only" trials (at 50% of maximum vibration level) for estimating the weights on the forward model (see below). All 12 possible stimuli (5 amplitude levels with mask absent, 5 amplitude conditions with target + mask, target-only, and mask-only) were presented five times in each run, along with five blank trials. This created a total of 65 trials per run (including blank trials), with 1 run lasting 5 min and 6 s. Stimuli were presented in randomly shuffled order, with interstimulus intervals (ISIs) of 3, 4.5, or 6 s (also in randomly shuffled order).

Subjects performed an asynchronous visual change-detection task continuously throughout each run, to maintain a consistent behavioral state and to divert attention away from the tactile stimuli (Fig. 1). In two intervals (500 ms each, ISI 500 ms), subjects were shown four small, randomly colored disks (size: 0.5° of visual angle, distance from fixation: 1° of visual angle). One of the disks changed color between intervals, and the subject's task was to indicate which one by means of a button press with one of the fingers of the left hand. Diverting attention away from the tactile target stimuli yielded a measure of the stimulus-evoked response that was not confounded with attentional modulation. Without any attentional control, we (and others) have reported large and highly variable (trial to trial) sensory-evoked responses in cortex (e.g., Ress et al. 2000).

Segmentation, cortical flattening, and delineation of regions of interest. For each subject, the high-resolution anatomical volume was segmented and computationally (Figs. 2 and 3) flattened with the public domain software FreeSurfer (Dale et al. 1999) and then automatically parcellated into human cortical gyri and sulci with an atlas of standardized nomenclature and criteria (Destrieux et al. 2010). From these labels, we created four regions of interest (ROIs): the pre- and postcentral gyrus of each hemisphere (Fig. 2). Most important of these four ROIs was the left postcentral gyrus, containing S1 contralateral to the stimulated hand. The remaining three ROIs served as controls.

Response time courses, response amplitudes, and response reliability. fMRI data were preprocessed with standard procedures. The first four images of each run were discarded to allow the longitudinal magnetization to reach steady state. We compensated for head movements within and across runs with a robust motion estima-
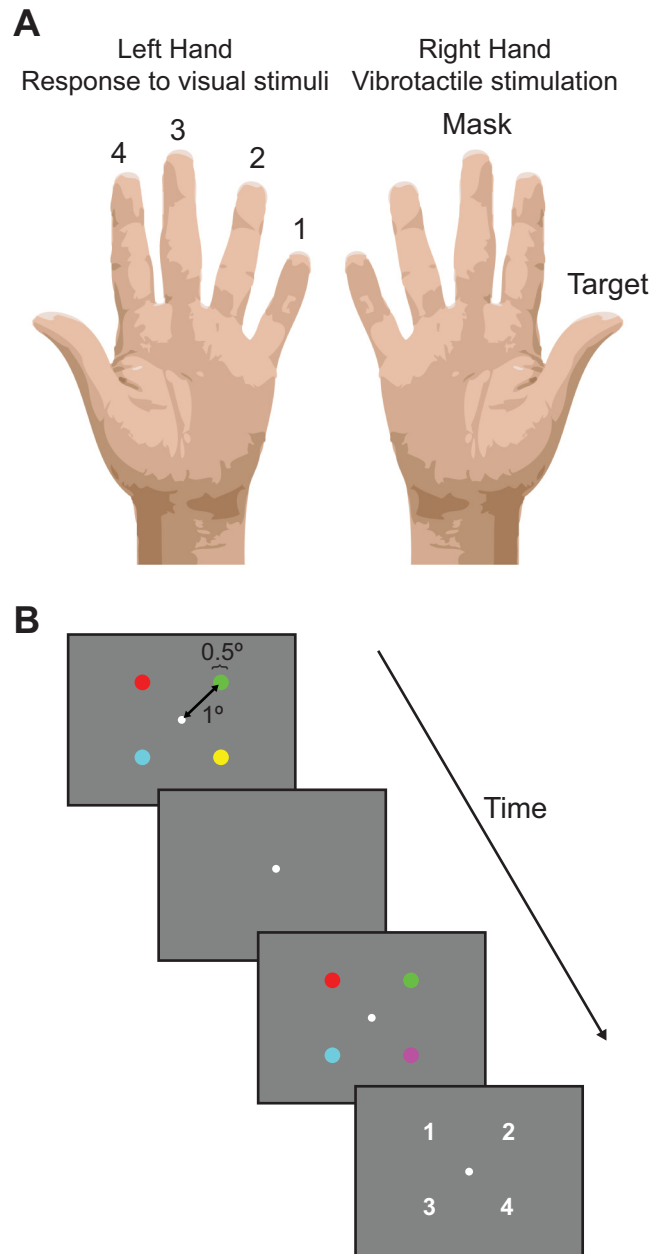

Fig. 1. Experiment design. *A*: vibrotactile stimulation was delivered to the right thumb (target stimulus) and right middle finger (mask stimulus). *B*: the visual task was a 2-interval change detection task. In the first interval (500 ms), 4 differently colored disks were presented around fixation. This was followed by a 500-ms interstimulus interval (ISI) and a second interval (500 ms) in which 1 of the 4 disks changed to a new random color. The subject was instructed to indicate which disk had changed in the subsequent response interval (1,000 ms), using the left-hand fingers to press 1 of 4 buttons.

tion algorithm (Nestares and Heeger 2000), divided the time series of each voxel by its mean image intensity to convert to percent signal change and compensate for distance from the RF coil, and linearly detrended and high-pass filtered the resulting time series with a cutoff frequency of 0.01 Hz to remove low-frequency drift. The hemodynamic impulse response function (HIRF) of each ROI was estimated with deconvolution (Dale 1999), with a procedure described in detail previously (Brouwer and Heeger 2009, 2011).

The response amplitudes for each trial type were measured separately for each voxel in each ROI and separately for each run, with linear regression. A regression matrix was constructed for each ROI
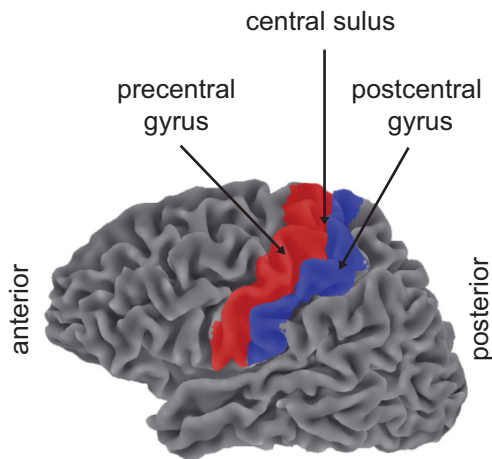
Fig. 2. Regions of interest (ROIs). Automated parcellation of human cortical gyri and sulci provided 4 ROIs: left and right hemisphere pre- and postcentral gyrus.

by convolving the estimated HIRF and its numerical derivative with binary time courses corresponding to the onsets of each of the 12 trial types (with 1s at each stimulus onset and 0s elsewhere). This resulted in a regression matrix with 24 columns: 12 columns for the HIRF convolved with each of the 12 stimulus onsets and 12 columns for the HIRF-derivative convolved with each of the stimulus onsets. Each column of the regression matrix was linearly detrended and high-pass filtered, identically to the preprocessing of the fMRI measurements. Response amplitudes were estimated by multiplying the pseudoinverse of this regression matrix with the measured (and preprocessed) fMRI response time courses. The values (beta weights) obtained for the derivative regressors were discarded after response amplitudes were estimated (Brouwer and Heeger 2009). We included the HIRF derivative in the regression, even though the associated beta weights were discarded, because the HIRF of an individual voxel may have differed from the estimated HIRF. The HIRF and its derivative are not mutually orthogonal, so including the derivative in the regression accounted for some of the variance in the measured response time courses and affected the response amplitudes associated with the HIRF. The variance of the estimated response amplitudes across runs was indeed smaller with the derivative included than without it. We

thus obtained, for each voxel and each run, one response amplitude measurement for each of the different trial types.

The activation of each voxel was quantified as the fraction of the variance in the original time course that was accounted for by the regression model, i.e., r^2 (Fig. 3A). A voxel with no repeatable response to the stimuli would have had $r^2 = 0$. A voxel whose time course consisted of identical responses to each stimulus presentation perfectly fit by the regression model would have had $r^2 = 1$.

Voxel selection. No statistical test was used to identify statistically active voxels, because our goal was not to localize somatosensory cortex but rather to measure and characterize the physiology in that cortical area. Instead, we simply selected voxels from each of the four ROIs (pre- and postcentral gyrus of each hemisphere) that showed the most reliable stimulus-evoked responses (Fig. 3A). Specifically, we included voxels with activation (r^2, variance in the original time course that was accounted for by the regression model) in the top 75th percentile, thus selecting 25% of the original voxels for the subsequent analysis. This split was arbitrary and was used solely to remove noisy voxels. A range of other thresholds (25th–75th percentiles) yielded similar results and supported the same conclusions.

Baseline removal. A baseline was removed from each voxel's response, separately for each run, in each scanning session. Specifically, let m be the number of voxels and c the number of conditions, resulting in a matrix of estimated response amplitudes **B** of size $m \times c$, for each run. For each **B**, we computed the mean responses across all stimulus conditions, yielding a vector **v** of mean response amplitudes of length m (1 per voxel). This vector was normalized to a unit vector and removed by linear projection: $\mathbf{B}^* = \mathbf{B} - (\mathbf{B}^T\mathbf{v})\mathbf{v}$. The baseline removal was done as an additional preprocessing step before transforming the voxel responses to the channel responses (described next). This analysis step was not performed when computing the mean responses across voxels.

Forward model. Following our previous work on color vision and cross-orientation suppression (Brouwer and Heeger 2009, 2011, 2013), we used a forward model to separate the voxel responses into two channel responses, selective for the thumb and middle finger. At the scale of individual neurons, the representations of the thumb and middle finger occupy different, but partially overlapping, subregions of the somatosensory cortex. Because of the overlap coupled with the limited resolution of our fMRI measurements (10 mm³), many voxels contained neurons responsive to both digits, in varying proportions. We defined two idealized channels, one responsive to only thumb
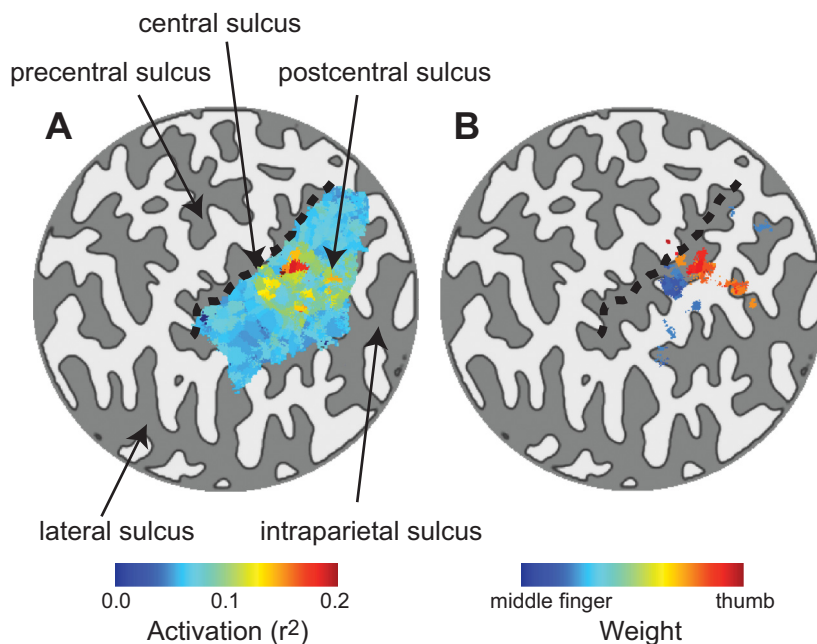

Fig. 3. Activation and weight maps. *A:* activation map: stimulus-evoked activation shown on a flattened representation (flat map) of the left hemisphere central sulcus for a typical example subject. Dark gray, sulci; light gray, gyri; colors, activation of each voxel in the postcentral gyrus ROI, quantified as the fraction of the variance in the original time course that was accounted for by the regression model (r^2). Dashed line indicates border between the post- and precentral gyri. *B:* weight map. Colors, weights assigned by the forward model to each voxel, rescaled to range from 0 to 1, for voxels with response reliability (from *A*) exceeding $r^2 > 0.1$.

stimulation and the other responsive to only middle finger stimulation. The responses of each voxel were assumed to be a weighted sum of the responses of these two channels. In the first stage of the analysis, we used the response amplitudes from the target-only and mask-only conditions to estimate the weights on the two hypothetical channels, separately for each voxel. With these weights in hand, the second stage of analysis computed the channel responses evoked by the mask-absent and target + mask trials, i.e., those in which we varied the amplitude of the target and the presence of the mask. Let m be the number of voxels and n the number of repeated measurements. The matrix of response amplitudes for the target-only and mask-only conditions ($\mathbf{B}_w$, $m \times n$) was related to the matrix of hypothetical channel responses ($\mathbf{C}_w$, $2 \times n$) by a weight matrix ($\mathbf{W}$, $m \times 2$):

$$\mathbf{B}_w = \mathbf{W}\mathbf{C}_w \tag{1}$$

The matrix of hypothetical channel responses $\mathbf{C}_w$ was a binary matrix with 2 rows (1 for each channel) and n columns (repeated measures). For the target-only stimuli, the first row was set to 1 and the second column was set to 0. For the mask-only stimuli, this was reversed. The least-squares estimate of the weights was computed with linear regression:

$$\hat{\mathbf{W}} = \mathbf{B}_w \mathbf{C}_w^T \left(\mathbf{C}_w \mathbf{C}_w^T \right)^{-1} \tag{2}$$

The channel responses to mask-absent and target + mask stimuli ($\mathbf{B}_c$) were then computed, again with linear regression:

$$\hat{\mathbf{C}}_c = (\hat{\mathbf{W}}^T \hat{\mathbf{W}})^{-1} \hat{\mathbf{W}}^T \mathbf{B}_c \tag{3}$$

For these matrices to be invertible, the number of voxels must be greater than the number of channels (2), and there must be an uneven weighting of these two channels in at least a subset of the voxels so that the voxels exhibit sufficiently different responses to stimulation of the two digits. These requirements posed no difficulty since the average size of our ROIs across subjects was ~100 voxels, and there were stable biases in the responses of voxels to different digits, as expected from the known organization of somatosensory cortex. The channel responses to each of the mask-absent and target + mask stimuli were computed separately for each subject, averaged across runs. Finally, we computed the grand mean and SE of the channel responses across subjects, separately for each stimulus condition.

Normalization model fit. The normalization model (Carandini and Heeger 2012) was used to fit the channel responses. The response of the target channel as a function of target and mask amplitude was modeled as

$$r_i = r_{max} \left(\frac{a_t^n}{\left(\sqrt{a_t^2 + a_m^2} \right)^n + \sigma^n} \right) + b \tag{4a}$$

Similarly, the response of the mask channel as a function of target and mask amplitude was modeled as

$$r_m = r_{max} \left(\frac{a_m^n}{\left(\sqrt{a_t^2 + a_m^2} \right)^n + \sigma^n} \right) + b \tag{4b}$$

where in both equations a_t is the target amplitude and a_m is the mask amplitude. The model had four parameters: σ, n, r_{max}, and b, determining the gain, slope, saturation and baseline of the response functions, respectively. We fitted the channel responses simultaneously, for all target amplitudes and for both mask-absent and target + mask stimulation. There were a total of 20 data points (2 channels, 5 target amplitudes, 2 mask amplitudes) to constrain the four parameters.

Gain change. To test for and quantify a shift in gain for target + mask compared with mask absent, we fitted a simplified version of the normalization model to the responses in the target channel:

$$r_t = r_{max} \left(\frac{a^n}{a^n + \sigma^n} \right) + b \tag{5}$$

For these fits, we fixed all parameters to the values obtained in the simultaneous fit described above, with the exception of σ, the parameter determining the gain of the response function. We fitted the response functions separately for the target + mask and mask-absent conditions, thereby obtaining a value of σ for each condition. If the presence of the mask led to a decrease in gain, the σ parameter for the target + mask condition would have been larger than the σ for the mask-absent condition (i.e., a stronger target amplitude would have been needed to achieve the same response).

The statistical significance of any difference in σ values was determined by means of bootstrapping. We randomly resampled the data, with replacement, and then fitted the model (*Eq. 5*) to the resampled data set. Repeating this procedure a large number of times provided distributions of σ parameter values that were statistically compared between conditions. Specifically, we computed the ratios between each pair of bootstrapped σ parameter values corresponding to the target + mask and mask-absent conditions. This generated a new distribution of σ ratios for which we determined the median and 5th and 95th percentiles. If the σ values were not statistically different, the distribution of their ratios would have been centered on 1, with the 5th percentile being smaller and the 95th percentile being larger than 1. If the 5th percentile was larger than 1, we concluded that there was a statistically significant change in gain (a 1-tailed test given the prior hypothesis that the mask should decrease the gain of responses to the target).

Mean responses. The normalization model was also fit to the mean responses, averaged across voxels in each ROI, rather than the channel responses. The goal of this analysis was to determine to what extent the mean responses reflected the underlying cross-digit suppression observed in the channel responses. The mean responses were fit with two models. The normalization model predicted cross-digit suppression, summing the responses of the target and mask channels (i.e., summing Eqs. 4a and 4b):

$$r = r_{max} \left(\frac{a_t^n + a_m^n}{\left(\sqrt{a_t^2 + a_m^2} \right)^n + \sigma^n} \right) + b \tag{6}$$

The alternative model did not have cross-digit suppression (only the target amplitude appears in the denominator of the first term and only the mask amplitude appears in the second term):

$$r = r_{max} \left(\frac{a_t^n}{a_t^n + \sigma^n} + \frac{a_m^n}{a_m^n + \sigma^n} \right) + b \tag{7}$$

These equations specifically modeled the average responses to the concurrent vibrotactile stimuli, rather than the responses of separate channels.

Statistical significance of the model fits was determined with cross-validation. We divided the data in half. Both models were fitted to the first half of the data. Using the resulting best-fit parameter values, we predicted the responses in the remaining half of the data and computed the variance explained by the predicted responses (r^2). Repeating this procedure a large number of times with different (random) subdivisions of the data generated distributions of r^2 values, one distribution for each model (with and without cross-digit suppression). Taking the ratio between these two distributions (r^2 model with cross-digit suppression:r^2 model without cross-digit suppression) generated a new distribution for which we determined the median and 5th and 95th percentiles. If the r^2 values were not statistically different, the distribution of their ratios would have been centered on 1, with the 5th percentile being smaller and the 95th percentile being larger than 1. If we found that the 5th percentile was larger than 1, we concluded that the model with cross-digit suppression provided a statistically better fit to the data than the model without cross-digit suppression. If,
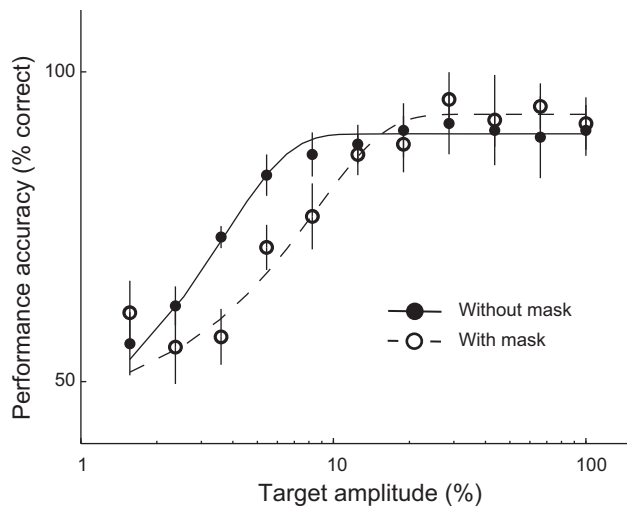
Fig. 4. Psychophysics. Subjects reported the stimulus interval containing vibrotactile stimulation to the thumb (target) as a function of target amplitude, with and without concurrent stimulation of the middle finger (mask). Filled symbols, target detection without mask; open symbols, target detection with mask. Error bars, SE across 5 subjects. Curves are maximum likelihood fits using Weibull functions.

on the other hand, the distribution of ratios yielded a 95th percentile smaller than 1, we concluded that the model without cross-digit suppression provided a statistically better fit to the data than the model with cross-digit suppression.

Psychophysics. We measured psychophysical cross-digit masking in a separate experiment (outside the scanner) using the same vibrotactile stimulator. In a two-interval forced-choice task (2IFC), subjects were presented with two stimuli (each for 375 ms) in which the target (thumb) was stimulated during one of the two intervals. Subjects pressed one of two buttons to indicate which interval contained target stimulation. Target (thumb) amplitude was varied across trials between 1.56% and 50% maximum amplitude (logarithmically spaced) in randomly shuffled order. Mask (middle finger) amplitude was either 0 (without mask) or 50% maximum amplitude in randomly shuffled order. Mask amplitude was identical on both intervals of each trial. Psychometric functions (% correct vs. target amplitude) were fit (maximum likelihood) with Weibull functions. The strength of cross-digit masking was measured as the change in target detection thresholds (75% correct) with and without the mask. Statistical significance of the threshold difference between the two conditions was determined by a randomization test.

RESULTS

Psychophysical evidence of cross-digit suppression. Subjects were less sensitive to somatosensory stimulation on the thumb when the thumb and middle finger were stimulated concurrently compared with when only the thumb was stimulated (Fig. 4). Target detection thresholds (75% correct responses) were higher when target and mask digits were stimulated concurrently compared with when the target was stimulated in isolation (Fig. 4; $P < 0.05$).

Activation and weight maps. Stimulation of the right thumb (target) and middle finger (mask) produced an expected pattern of activity in the left postcentral gyrus (Fig. 3). Clusters of active voxels were found at the known location of the somatosensory representation of these digits (Fig. 3A). Replicating previous reports (Besle et al. 2013, 2014; Francis et al. 2000; Nelson and Chen 2008; Sanchez-Panchuelo et al. 2010;

Schweizer et al. 2008; Stringer et al. 2011), we observed considerable overlap between the responses to the target and mask. Despite the overlap, there were two clusters of activity, one with a bias for the middle finger and the other with a bias for the thumb (Fig. 3B). The fMRI responses were fit with a model in which it was assumed that each voxel's responses were a weighted sum of the responses of two hypothetical channels, selective for the thumb and middle finger. These weights were estimated, separately for each voxel, based on the response amplitudes from the target-only and mask-only conditions. The weights were then rescaled to range from 0 to 1. Values close to 0 indicated that the responses in a voxel were dominated by stimulation to the middle finger (Fig. 3B), while values close to 1 indicated that the responses were dominated by stimulation to the thumb (Fig. 3B). The region of cortex between these two clusters responded to both thumb and middle finger stimulation, and part of this region presumably would have responded preferentially to index finger stimulation.

Cross-digit suppression in somatosensory cortex. To measure cross-digit suppression, a target stimulus was presented to the thumb at five different amplitude levels either in isolation (mask absent) or concurrent with a mask stimulus presented to the middle finger (target + mask). In addition, we included the separate mask-only and target-only trials (as mentioned above) for estimating the channel weights. Because of overlap between the representations of the target and mask digits, we could not define distinct subregions that responded to only one but not the other digit. Instead, we used a forward model to separate the cortical activity evoked by the two digits by transforming the fMRI measurements from the voxel responses into channel responses. Again, the responses of each voxel were assumed to be a weighted sum of the responses of two channels, selective for thumb and middle finger. In the first stage of the analysis, we used the response amplitudes from the target-only and mask-only conditions to estimate the weights on the two hypothetical channels, separately for each voxel. With these weights in hand, the second stage of analysis computed the channel responses evoked by the mask-absent and target + mask trials, i.e., those in which we varied the amplitude of the target and the presence of the mask.

fMRI responses in the left postcentral gyrus ROI exhibited cross-digit suppression (Fig. 5, A and B). For the channel tuned to the target (thumb), responses increased with target stimulus amplitude when the mask was absent (Fig. 5A). This response function was shifted rightward on the log-amplitude axis in the presence of the mask (Fig. 5A). This rightward shift on the log axis is the hallmark of divisive normalization. The channel preferring the mask digit exhibited a constant "baseline" response to target stimulation regardless of target amplitude (Fig. 5B). The mask channel responded strongly to the mask stimulus, and its responses to the mask decreased with increasing amplitude of the concurrently presented target (Fig. 5B).

As a control, we also analyzed data from each of the other three ROIs. As expected, the target- and mask-specific channels from right hemisphere postcentral gyrus (ipsilateral to the stimulation) exhibited weak, if any, stimulus-evoked responses and little, if any, evidence of suppression (Fig. 5, C and D). Similar results were observed for the right precentral gyrus (data not shown). The left precentral gyrus did show some stimulus-evoked responses and evidence of suppression, albeit
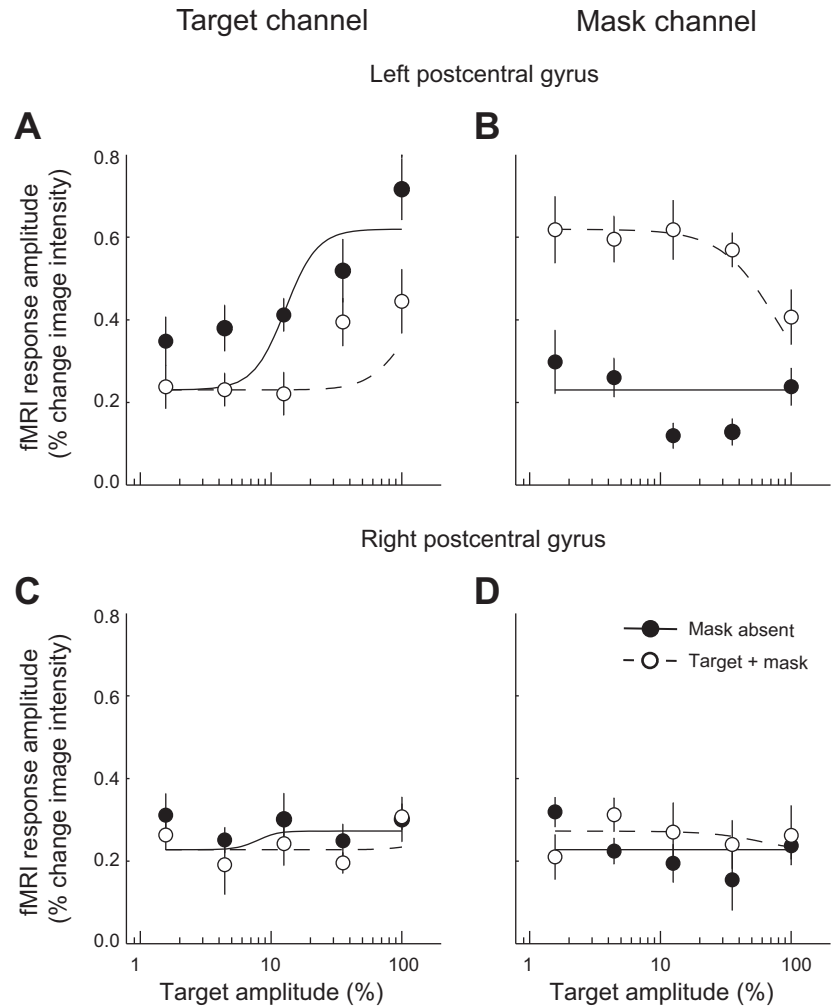
Fig. 5. Cross-digit suppression in human somatosensory cortex. *A* and *B*: channel responses from left hemisphere postcentral gyrus. *C* and *D*: right hemisphere postcentral gyrus. *A* and *C*: channel selective for thumb (target) stimulation. *B* and *D*: channel selective for middle finger (mask) stimulation. Filled symbols, mask absent; open symbols, target + mask. Error bars, SE across 6 subjects. Dashed and solid curves, normalization model.

weaker than those observed in the left postcentral gyrus. This might be explained by partial voluming of the fMRI measurements: voxels assigned to the precentral gyrus ROI might have extended into postcentral gyrus, because of folding of the cortical surface. Another possibility is that responses in the precentral gyrus reflected activity of genuine sensory neurons, which are in fact scattered throughout motor cortex (Penfield and Erickson 1941). A third explanation is that motor neurons in precentral gyrus might have received input from their counterparts (i.e., representing the same body part) in somatosensory cortex (postcentral gyrus).

Normalization model fit. We fitted the responses from both channels and both conditions (target + mask, mask absent) with the normalization model (Eqs. 4a and 4b). The normalization model had four free parameters, σ, n, r_{max}, and b, that determined the amplitude gain, slope, saturation, and baseline of the response functions, respectively. Cross-digit suppression is predicted by the normalization model because both target amplitude and mask amplitude appear in the denominators of the equations (Eqs. 4a and 4b). Increasing the mask amplitude causes the response of the target channel to decrease, and vice versa. The dashed and solid curves in Fig. 5 represent the best fit. For the left postcentral gyrus, the normalization model provided a good fit to the channel responses (model fit $r^2 = 0.85$). The best-fit gain was $\sigma = 0.05$, and the best-fit exponent was $n = 2.23$.

For the right hemisphere postcentral gyrus, the fit of the normalization model was poor ($r^2 = 0.18$), as well as for the right hemisphere precentral gyrus ($r^2 = 0.25$). The fit of the model to the channel responses from left hemisphere precentral gyrus was reasonable ($r^2 = 0.61$), although still worse than left hemisphere postcentral gyrus.

Fitting the channel responses with the normalization model was considerably better than attempting to fit the model to voxel responses. Because of overlap between the representations of the target and mask digits, we could not define distinct ROIs that responded exclusively to only one digit. But, as noted above, there were two clusters of activity, one with a bias for the middle finger and the other with a bias for the thumb (Fig. 3*B*). These two voxel clusters in the left postcentral gyrus were used in an attempt to quantify the effect of the mask on the target, without using the forward model. We measured response amplitudes within each of these two clusters of voxels and fit these measurements with the normalization model (Eqs. 4a and 4b). This more conventional approach to the analysis resulted in qualitatively similar, but quantitatively inferior, results (data not shown); the fit to the target and mask ROI responses ($r^2 = 0.52$) was worse than the fit to the target and mask channel responses ($r^2 = 0.85$, same as reported above), using the same model.

Gain change. The suppression in the target channel during cross-digit suppression was due to a change in gain (Fig. 5*A*, rightward shift on log amplitude axis, i.e., change in σ). We fitted the responses in this channel to each condition (target + mask, mask absent) separately, using a simplified version of the normalization model, allowing σ to differ between conditions (*Eq. 5*). For the left postcentral gyrus ROI, the change in the target channel responses from the mask-absent to the target + mask condition was associated with a highly significant increase in the best-fit σ parameter value (mask absent $\sigma = 0.06$; target + mask $\sigma = 0.60$; $P < 0.001$, nonparametric test based on bootstrap distributions of σ parameter values).

For the left precentral gyrus ROI, there was weaker, but still significant, evidence for a difference in gain between the two conditions (mask absent $\sigma = 0.14$; target + mask $\sigma = 0.45$; $P < 0.01$). For the remaining two ROIs, we did not find strong evidence for a difference in gain between the two conditions, as expected given that the stimulus-evoked responses were weak or absent in those ROIs (right precentral gyrus $P = 0.05$; right postcentral gyrus $P = 0.06$).

Mean response amplitudes. The mean voxel responses also exhibited evidence for normalization, averaged across responsive voxels in each ROI, but not as clearly as in the channel responses (Fig. 6*A*). If there were no suppression, then the mean voxel responses to the target + mask stimuli would have been simply the sum of the responses to the target stimuli (of various amplitudes) plus the response to the mask stimulus. Therefore, the response function for the target + mask condition would have been shifted upward relative to the no-mask condition, with the same slope. However, the response functions were found to have different slopes and to converge at higher amplitudes, as predicted by the normalization model. We fit the normalization model to the mean voxel responses (*Eq. 6*) and compared it (using cross-validation, see MATERIALS AND METHODS) to an alternative model that was similar in all other respects but did not predict cross-digit suppression (*Eq. 7*). The fit with the normalization model was slightly better than that with the alternative model (normalization model $r^2 = 0.72$; alternative model $r^2 = 0.69$; $P < 0.001$, cross-validation).

Again, there was no evidence for normalization in the right hemisphere postcentral gyrus, ipsilateral to the stimulation, because there was little, if any, stimulus-evoked activity (Fig. 6*B*). Similar results were observed for the two remaining ROIs: the left and right precentral gyri (data not shown).

DISCUSSION

Normalization in somatosensory cortex. Using fMRI and forward modeling, we measured the activity in two hypothetical channels, each tuned to one of the two stimulated digits, and fit these digit-selective responses with the normalization model. We found clear evidence of cross-digit suppression. The normalization model provided a good fit to the response functions with and without the mask stimulus. The cross-digit suppression observed in the left postcentral gyrus correlated with the psychophysical data: concurrent vibrotactile stimulation to the middle finger masked the stimulation to the thumb, resulting in higher detection thresholds. These results are in line with earlier EEG (Gandevia et al. 1983), MEG (Hoechstetter et al. 2001), and fMRI (Krause et al. 2001; Kurth et al.

Mean responses
(averaged across voxels)

A Left postcentral gyrus
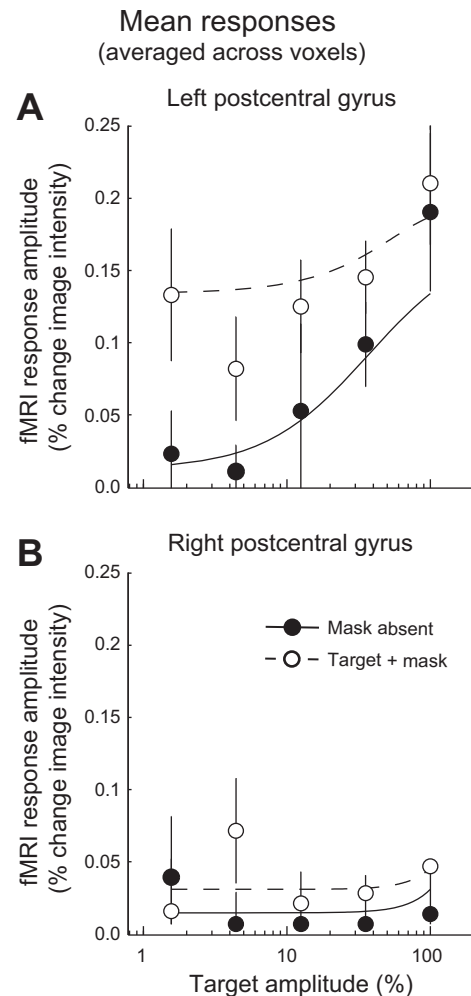
B Right postcentral gyrus

Fig. 6. Mean response amplitudes. *A*: mean response amplitudes, averaged across responsive voxels in the left hemisphere postcentral gyrus ROI. *B*: right hemisphere postcentral gyrus. Filled symbols, mask absent; open symbols, target + mask. Error bars, SE across 6 subjects. Dashed and solid curves, normalization model with cross-digit suppression.

2000; Ruben et al. 2006) studies that investigated the suppressive effects of concurrent tactile stimulation. In this study we used a novel methodology to further characterize the neural responses reflecting these suppressive effects and fit them with a computational model: divisive normalization.

Our results show that the normalization model can explain suppression of somatosensory responses from concurrent stimulation of different digits, adding to the growing body of evidence that divisive normalization is a canonical neural computation (Carandini and Heeger 2012). The normalization model was initially proposed to explain stimulus-evoked responses of individual neurons in V1 and has since been applied to explain neural activity in a wide variety of neural systems (see introduction for references). It has been argued that normalization provides a variety of useful functions including maximizing sensitivity for some stimulus features while maintaining invariance with respect to other stimulus dimensions. For example, normalization in V1 discards information about contrast to encode image pattern (e.g., orientation) (Albrecht and Hamilton 1982; Busse et al. 2009; Heeger 1992), optimizing discriminability regardless of contrast (Ringach 2010). It

has also been suggested that normalization in V1 improves the efficiency of sensory coding (Schwartz and Simoncelli 2001; Sinz and Bethge 2013; Wainwright et al. 2002). Analogous principles apply to somatosensory coding in S1.

Negative BOLD. We suggest that the response decrease that we observed in the presence of the mask stimulus reflected a suppression of neural responses, but our results might have been confounded by the hemodynamics. Target and mask stimulation evoked hemodynamic responses in adjacent and partially overlapping cortical regions. To satisfy the need for oxygenated blood in regions representing the mask digit, blood flow may have been diverted from the region representing the target digit, thereby reducing the fMRI responses evoked by the target, but without a concomitant decrease in neural activity. Indeed, it has been observed that an increase in fMRI responses in one region of visual or somatosensory cortex can be accompanied by a sustained decrease in fMRI responses (called "negative BOLD") in both neighboring brain regions, and also in the contralateral hemisphere (Blankenburg et al. 2003b; Devor et al. 2007; Harel et al. 2002; Hlushchuk and Hari 2006; Kastrup et al. 2008; Logothetis 2002; Raichle et al. 2001; Shmuel et al. 2002, 2006; Shmuel and Leopold 2008; Smith et al. 2004; Tootell et al. 1998; Wade and Rowland 2010). It has also been suggested that negative BOLD might be partially due to hemodynamics (Harel et al. 2002; Shmuel et al. 2002; Woolsey et al. 1996). However, the consensus of evidence indicates that negative BOLD reflects a decrease in neural activity below baseline (Devor et al. 2007; Kastrup et al. 2008; Shmuel et al. 2006; Shmuel and Leopold 2008; Smith et al. 2004; Tootell et al. 1998; Wade and Rowland 2010). Nevertheless, we must consider the possibility that a hemodynamic effect might have contributed to our results in addition to neural suppression.

To distinguish between neural and hemodynamic effects in visual cortical areas, we (and others) have used the difference in the timescale of these effects, with neural suppression being much faster (Brouwer and Heeger 2011; Kastner et al. 2001; Zenger-Landolt and Heeger 2003). Specifically, we ran control experiments in which the mask stimulus appeared with a lag, after the target disappeared. This lag was long enough to abolish the psychophysical masking effect of the mask, and there was no evidence of suppression in the fMRI responses. These results thereby favored the neural suppression interpretation, with no evidence for a hemodynamic confound. We considered running the analogous control experiment in the present study but chose not to do so because *1*) there was little reason to suspect that the hemodynamics in S1 is markedly different from that in each of several areas of visual cortex; *2*) the negative BOLD findings in S1 are directly analogous to those in V1; and *3*) it has already been reported with EEG and MEG that concurrent stimulation of the fingertips suppressed responses compared with sequential stimulation of the same fingertips (Gandevia et al. 1983; Hoechstetter et al. 2001).

Forward model. We (and others) have previously shown that the forward model is a useful tool to extract and isolate responses corresponding to subpopulations of neurons with different selectivities from an ensemble measure of neural activity (Anderson et al. 2013, 2014; Brouwer and Heeger 2009, 2011, 2013; Ester et al. 2013; Garcia et al. 2013; Ho et al. 2012; Kay et al. 2008; Kok et al. 2013; Saproo and Serences 2014; Scolari et al. 2012; Serences and Saproo 2012). The

forward model thereby offers an approach for analyzing the ensemble activity of large populations of neurons, to test computational theories of brain function (such as divisive normalization). The method can be applied not only to fMRI but also to optical imaging (intrinsic hemodynamic imaging, voltage-sensitive dye imaging, wide-field calcium imaging), EEG, MEG, intracortical EEG (ECoG), local field potentials, and multiunit spiking.

For the present experiment, we did not assume that neurons selective for the different digits were spatially segregated at the resolution of our measurements. Representations of the thumb and middle finger occupy different, but partially overlapping, subregions of the somatosensory cortex (see introduction for references). Individual neurons within both subregions may respond to both digits, in varying proportions. In addition, because of the limited resolution of our fMRI measurements (10 mm³), many voxels were likely to contain neurons responsive to both digits. The advantage of the forward model is its ability to separate responses to stimulation of different digits from voxels that do not show a complete bias to one digit or the other. Therefore, if two or more stimuli evoke overlapping neural representations (i.e., somatosensory stimulation to different digits, visual stimuli differing in orientation, motion direction, color, object class), the forward model provides a tool to separate their contributions and to quantify how they interact when presented concurrently. For comparison to the forward model, we tried to separate the responses of two distinct clusters of voxels, one with a bias for the middle finger and the other with a bias for the thumb. This approach produced qualitatively similar, but quantitatively inferior, results. We also analyzed the mean fMRI responses, averaged over all responsive voxels; the channel responses determined with the forward model exhibited clear changes in gain with concurrent mask stimulation that were not (and not expected to be) evident in the mean voxel responses.

Possible extensions. S1 can be divided into distinct subregions (3a, 3b, 1, and 2), raising the question of whether normalization in S1 differs across these subregions. Electrophysiology studies in nonhuman primates have demonstrated an anterior-to-posterior somatotopic organization corresponding to the proximal-to-distal (base to tip) surface of each finger (Kaas et al. 1979; Merzenich et al. 1978; Paul et al. 1972). The representation in each subregion of S1 mirrors the representation in the adjacent area (i.e., base to tip is posterior to anterior in area 3b but anterior to posterior in area 1). This layout results in map reversals of representations at the boundaries between areas 3a, 3b, 1, and 2 (Darian-Smith 1982). Analogous subdivisions of human S1 have been reported based on cytoarchitectonic differences in postmortem brains (Geyer et al. 1997, 1999, 2000). Most previous human fMRI studies have attempted to assign functionally significant clusters of voxels to cytoarchitectonic areas based on anatomical criteria (Moore et al. 2000; Nelson and Chen 2008; Overduin and Servos 2008; Schweizer et al. 2008; Stringer et al. 2011), but considerable individual differences in somatotopic maps have been reported in both human and monkey S1 (Besle et al. 2013; Merzenich et al. 1987; Sanchez-Panchuelo et al. 2012) and there is considerable variability across individuals in the correspondence between cytoarchitectonic boundaries and the anatomical criteria (Geyer et al. 1999). A few fMRI studies have investigated within-finger somatotopy in human S1 (Blankenburg et al.

2003a; Overduin and Servos 2004, 2008; Schweisfurth et al. 2011), but only one study has succeeded in revealing the full sequence of map reversals in individual subjects, thereby clearly delineating distinct subregions of S1 (Sanchez-Panchuelo et al. 2012). That study used a 7-T MRI scanner to achieve sufficiently high spatial resolution (1.25 $\times$ 1.25 $\times$ 1.3-mm voxels), spatial specificity, and contrast-to-noise ratio (Gati et al. 1997; Yacoub et al. 2001). Consequently, to characterize normalization separately in each subregion of human S1 would require combining our present experiment and within-finger somatotopy in individual subjects using 7-T fMRI.

Of particular interest would be to determine whether interdigit suppression is evident in the subregions of S1 in which each neuron responds to only one digit, whether normalization is stronger in subregions of S1 that have neurons with larger receptive fields encompassing more than one digit, and whether normalization is stronger in subregions of S1 that respond equally to both digits. The forward model approach to the data analysis can be applied only when there is an uneven weighting of the two channels in at least a subset of the voxels, so that the voxels exhibit sufficiently different responses to stimulation of the two digits (see MATERIALS AND METHODS). For this reason, some of these questions will require a different approach.

Normalization has been found to interact with attention in visual cortex (Herrmann et al. 2010; Itthipuripat et al. 2014; Reynolds and Heeger 2009; Sundberg et al. 2009), so interdigit suppression might likewise depend on attention. In this experiment, we deliberately diverted attention away from the tactile stimuli by having subjects perform a simultaneous visual task. In this way we were able to measure stimulus-evoked responses not confounded by attentional modulation, and therefore more likely to reflect innate and fundamental perceptual processes. Cuing subjects to attend to one (or the other) of the vibrotactile stimuli, analogous to what has been done in V1, would provide a further test of the normalization model in S1.

The normalization model, which fit our results, may not apply to more complex tactile stimuli, or more generally to teleological high-value tasks such as grasping. The tactile stimuli in this study consisted exclusively of 1.5-s bursts of sinusoidally modulated 25-Hz vibration or "flutter" at various intensities (i.e., amplitudes). Normal grasping involves, in fact depends on, attention, volitional movement, sensorimotor integration across at least two digits and at least eight joints, and vision. The present experiment deliberately excluded all of these variables, to allow us to test the hypothesis that tactile masking of flutter stimuli can be explained by the normalization model. Our results, taken together, imply that somatosensory discrimination (psychophysical thresholds) should be worse when grasping an object vs. touching one finger to the surface of the object. This prediction has not been tested. We can speculate, however, that since normalization appears to be a canonical computation performed on sensory inputs of multiple modalities to produce information of teleological value, it is likely to play a role in the computations underlying the grasping process. More specifically, as with nearly all volitional behaviors, grasping requires that task-dependent sensory stimuli be made salient relative to the flood of simultaneous and multimodal task-independent stimuli. To the extent that the normalization computations can account for masking, it is at least conceivable that the same process underlies task-dependent stimulus saliency. Whether the normalization model in fact generalizes to neuronal responses to other types of tactile stimuli, or to complex tasks, will require additional experiments.

DISCLOSURES

No conflicts of interest, financial or otherwise, are declared by the author(s).

AUTHOR CONTRIBUTIONS

Author contributions: G.J.B., D.J.H., and A.C.G. conception and design of research; G.J.B., V.A., and S.O. performed experiments; G.J.B. and S.O. analyzed data; G.J.B. and D.J.H. interpreted results of experiments; G.J.B. and S.O. prepared figures; G.J.B., S.O., and D.J.H. drafted manuscript; G.J.B., D.J.H., and A.C.G. edited and revised manuscript; G.J.B., S.O., D.J.H., and A.C.G. approved final version of manuscript.

REFERENCES

Albrecht DG, Hamilton DB. Striate cortex of monkey and cat: contrast response function. *J Neurophysiol* 48: 217–237, 1982.

Anderson DE, Ester EF, Serences JT, Awh E. Attending multiple items decreases the selectivity of population responses in human primary visual cortex. *J Neurosci* 33: 9273–9282, 2013.

Anderson DE, Serences JT, Vogel EK, Awh E. Induced alpha rhythms track the content and quality of visual working memory representations with high temporal precision. *J Neurosci* 34: 7587–7599, 2014.

Besle J, Sanchez-Panchuelo RM, Bowtell R, Francis S, Schluppeck D. Event-related fMRI at 7T reveals overlapping cortical representations for adjacent fingertips in S1 of individual subjects. *Hum Brain Mapp* 35: 2027–2043, 2014.

Besle J, Sanchez-Panchuelo RM, Bowtell R, Francis S, Schluppeck D. Single-subject fMRI mapping at 7 T of the representation of fingertips in S1: a comparison of event-related and phase-encoding designs. *J Neurophysiol* 109: 2293–2305, 2013.

Blankenburg F, Ruben J, Meyer R, Schwiemann J, Villringer A. Evidence for a rostral-to-caudal somatotopic organization in human primary somatosensory cortex with mirror-reversal in areas 3b and 1. *Cereb Cortex* 13: 987–993, 2003a.

Blankenburg F, Taskin B, Ruben J, Moosmann M, Ritter P, Curio G, Villringer A. Imperceptible stimuli and sensory processing impediment. *Science* 299: 1864, 2003b.

Brouwer GJ, Heeger DJ. Decoding and reconstructing color from responses in human visual cortex. *J Neurosci* 29: 13992–14003, 2009.

Brouwer GJ, Heeger DJ. Cross-orientation suppression in human visual cortex. *J Neurophysiol* 106: 2108–2119, 2011.

Brouwer GJ, Heeger DJ. Categorical clustering of the neural representation of color. *J Neurosci* 33: 15454–15465, 2013.

Busse L, Wade AR, Carandini M. Representation of concurrent stimuli by population activity in visual cortex. *Neuron* 64: 931–942, 2009.

Carandini M, Heeger DJ. Summation and division by neurons in primate visual cortex. *Science* 264: 1333–1336, 1994.

Carandini M, Heeger DJ. Normalization as a canonical neural computation. *Nat Rev Neurosci* 13: 51–62, 2012.

Carandini M, Heeger DJ, Movshon JA. Linearity and normalization in simple cells of the macaque primary visual cortex. *J Neurosci* 17: 8621–8644, 1997.

Cavanaugh JR, Bair W, Movshon JA. Nature and interaction of signals from the receptive field center and surround in macaque V1 neurons. *J Neurophysiol* 88: 2530–2546, 2002a.

Cavanaugh JR, Bair W, Movshon JA. Selectivity and spatial distribution of signals from the receptive field surround in macaque V1 neurons. *J Neurophysiol* 88: 2547–2556, 2002b.

Dale AM. Optimal experimental design for event-related fMRI. *Hum Brain Mapp* 8: 109–114, 1999.

Dale AM, Fischl B, Sereno MI. Cortical surface-based analysis. I. Segmentation and surface reconstruction. *Neuroimage* 9: 179–194, 1999.

Darian-Smith I. Touch in primates. *Annu Rev Psychol* 33: 155–194, 1982.

DeAngelis GC, Robson JG, Ohzawa I, Freeman RD. The organization of suppression in receptive fields of neurons in the cat's visual cortex. *J Neurophysiol* 68: 144–163, 1992.

Destrieux C, Fischl B, Dale A, Halgren E. Automatic parcellation of human cortical gyri and sulci using standard anatomical nomenclature. *Neuroimage* 53: 1–15, 2010.

Devor A, Tian P, Nishimura N, Teng IC, Hillman EM, Narayanan SN, Ulbert I, Boas DA, Kleinfeld D, Dale AM. Suppressed neuronal activity and concurrent arteriolar vasoconstriction may explain negative blood oxygenation level-dependent signal. *J Neurosci* 27: 4452–4459, 2007.

Ester EF, Anderson DE, Serences JT, Awh E. A neural measure of precision in visual working memory. *J Cogn Neurosci* 25: 754–761, 2013.

Foley JM. Human luminance pattern-vision mechanisms: masking experiments require a new model. *J Opt Soc Am A* 11: 1710–1719, 1994.

Francis ST, Kelly EF, Bowtell R, Dunseath WJ, Folger SE, McGlone F. fMRI of the responses to vibratory stimulation of digit tips. *Neuroimage* 11: 188–202, 2000.

Gandevia SC, Burke D, McKeon BB. Convergence in the somatosensory pathway between cutaneous afferents from the index and middle fingers in man. *Exp Brain Res* 50: 415–425, 1983.

Garcia JO, Srinivasan R, Serences JT. Near-real-time feature-selective modulations in human cortex. *Curr Biol* 23: 515–522, 2013.

Gardner EP, Spencer WA. Sensory funneling. I. Psychophysical observations of human subjects and responses of cutaneous mechanoreceptive afferents in the cat to patterned skin stimuli. *J Neurophysiol* 35: 925–953, 1972a.

Gardner EP, Spencer WA. Sensory funneling. II. Cortical neuronal representation of patterned cutaneous stimuli. *J Neurophysiol* 35: 954–977, 1972b.

Gati JS, Menon RS, Ugurbil K, Rutt BK. Experimental determination of the BOLD field strength dependence in vessels and tissue. *Magn Reson Med* 38: 296–302, 1997.

Geisler WS, Albrecht DG. Cortical neurons: isolation of contrast gain control. *Vision Res* 32: 1409–1410, 1992.

Geyer S, Schleicher A, Zilles K. The somatosensory cortex of human: cytoarchitecture and regional distributions of receptor-binding sites. *Neuroimage* 6: 27–45, 1997.

Geyer S, Schleicher A, Zilles K. Areas 3a, 3b, and 1 of human primary somatosensory cortex. *Neuroimage* 10: 63–83, 1999.

Geyer S, Schormann T, Mohlberg H, Zilles K. Areas 3a, 3b, and 1 of human primary somatosensory cortex. Part 2. Spatial normalization to standard anatomical space. *Neuroimage* 11: 684–696, 2000.

Harel N, Lee SP, Nagaoka T, Kim DS, Kim SG. Origin of negative blood oxygenation level-dependent fMRI signals. *J Cereb Blood Flow Metab* 22: 908–917, 2002.

Heeger DJ. Normalization of cell responses in cat striate cortex. *Vis Neurosci* 9: 181–197, 1992.

Heeger DJ, Simoncelli EP, Movshon JA. Computational models of cortical visual processing. *Proc Natl Acad Sci USA* 93: 623–627, 1996.

Herrmann K, Montaser-Kouhsari L, Carrasco M, Heeger DJ. When size matters: attention affects performance by contrast or response gain. *Nat Neurosci* 13: 1554–1559, 2010.

Hlushchuk Y, Hari R. Transient suppression of ipsilateral primary somatosensory cortex during tactile finger stimulation. *J Neurosci* 26: 5819–5824, 2006.

Ho T, Brown S, van Maanen L, Forstmann BU, Wagenmakers EJ, Serences JT. The optimality of sensory processing during the speed-accuracy tradeoff. *J Neurosci* 32: 7992–8003, 2012.

Hoechstetter K, Rupp A, Stancak A, Meinck HM, Stippich C, Berg P, Scherg M. Interaction of tactile input in the human primary and secondary somatosensory cortex—a magnetoencephalographic study. *Neuroimage* 14: 759–767, 2001.

Hyvarinen J, Poranen A. Receptive field integration and submodality convergence in the hand area of the post-central gyrus of the alert monkey. *J Physiol* 283: 539–556, 1978.

Itthipuripat S, Garcia JO, Rungratsameetaweemana N, Sprague TC, Serences JT. Changing the spatial scope of attention alters patterns of neural gain in human cortex. *J Neurosci* 34: 112–123, 2014.

Iwamura Y, Tanaka M, Sakamoto M, Hikosaka O. Converging patterns of finger representation and complex response properties of neurons in area 1 of the first somatosensory cortex of the conscious monkey. *Exp Brain Res* 51: 327–337, 1983a.

Iwamura Y, Tanaka M, Sakamoto M, Hikosaka O. Functional subdivisions representing different finger regions in area 3 of the first somatosensory cortex of the conscious monkey. *Exp Brain Res* 51: 315–326, 1983b.

Kaas JH, Nelson RJ, Sur M, Lin CS, Merzenich MM. Multiple representations of the body within the primary somatosensory cortex of primates. *Science* 204: 521–523, 1979.

Kastner S, De Weerd P, Pinsk MA, Elizondo MI, Desimone R, Ungerleider LG. Modulation of sensory suppression: implications for receptive field sizes in the human visual cortex. *J Neurophysiol* 86: 1398–1411, 2001.

Kastrup A, Baudewig J, Schnaudigel S, Huonker R, Becker L, Sohns JM, Dechent P, Klingner C, Witte OW. Behavioral correlates of negative BOLD signal changes in the primary somatosensory cortex. *Neuroimage* 41: 1364–1371, 2008.

Kay KN, Naselaris T, Prenger RJ, Gallant JL. Identifying natural images from human brain activity. *Nature* 452: 352–355, 2008.

Kok P, Brouwer GJ, van Gerven MA, de Lange FP. Prior expectations bias sensory representations in visual cortex. *J Neurosci* 33: 16275–16284, 2013.

Krause T, Kurth R, Ruben J, Schwiemann J, Villringer K, Deuchert M, Moosmann M, Brandt S, Wolf K, Curio G, Villringer A. Representational overlap of adjacent fingers in multiple areas of human primary somatosensory cortex depends on electrical stimulus intensity: an fMRI study. *Brain Res* 899: 36–46, 2001.

Kurth R, Villringer K, Curio G, Wolf KJ, Krause T, Repenthin J, Schwiemann J, Deuchert M, Villringer A. fMRI shows multiple somatotopic digit representations in human primary somatosensory cortex. *Neuroreport* 11: 1487–1491, 2000.

Logothetis NK. The neural basis of the blood-oxygen-level-dependent functional magnetic resonance imaging signal. *Philos Trans R Soc Lond B Biol Sci* 357: 1003–1037, 2002.

Louie K, Glimcher PW. Separating value from choice: delay discounting activity in the lateral intraparietal area. *J Neurosci* 30: 5498–5507, 2010.

Louie K, Glimcher PW. Efficient coding and the neural representation of value. *Ann NY Acad Sci* 1251: 13–32, 2012.

Merzenich MM, Kaas JH, Sur M, Lin CS. Double representation of the body surface within cytoarchitectonic areas 3b and 1 in "SI" in the owl monkey (*Aotus trivirgatus*). *J Comp Neurol* 181: 41–73, 1978.

Merzenich MM, Nelson RJ, Kaas JH, Stryker MP, Jenkins WM, Zook JM, Cynader MS, Schoppmann A. Variability in hand surface representations in areas 3b and 1 in adult owl and squirrel monkeys. *J Comp Neurol* 258: 281–296, 1987.

Moore CI, Stern CE, Corkin S, Fischl B, Gray AC, Rosen BR, Dale AM. Segregation of somatosensory activation in the human rolandic cortex using fMRI. *J Neurophysiol* 84: 558–569, 2000.

Moradi F, Heeger DJ. Inter-ocular contrast normalization in human visual cortex. *J Vis* 9: 13.1–13.22, 2009.

Morrone MC, Burr DC. Evidence for the existence and development of visual inhibition in humans. *Nature* 321: 235–237, 1986.

Morrone MC, Burr DC, Maffei L. Functional implications of cross-orientation inhibition of cortical visual cells. *Proc R Soc Lond B Biol Sci* 216: 335–354, 1982.

Nelson AJ, Chen R. Digit somatotopy within cortical areas of the postcentral gyrus in humans. *Cereb Cortex* 18: 2341–2351, 2008.

Nestares O, Heeger DJ. Robust multiresolution alignment of MRI brain volumes. *Magn Reson Med* 43: 705–715, 2000.

Ogawa S, Lee TM, Kay AR, Tank DW. Brain magnetic resonance imaging with contrast dependent on blood oxygenation. *Proc Natl Acad Sci USA* 87: 9868–9872, 1990.

Ohshiro T, Angelaki DE, Deangelis GC. A normalization model of multisensory integration. *Nat Neurosci* 14: 775–782, 2011.

Olsen SR, Bhandawat V, Wilson RI. Divisive normalization in olfactory population codes. *Neuron* 66: 287–299, 2010.

Overduin SA, Servos P. Distributed digit somatotopy in primary somatosensory cortex. *Neuroimage* 23: 462–472, 2004.

Overduin SA, Servos P. Symmetric sensorimotor somatotopy. *PLoS One* 3: e1505, 2008.

Paul RL, Merzenich M, Goodman H. Representation of slowly and rapidly adapting cutaneous mechanoreceptors of the hand in Brodmann's areas 3 and 1 of *Macaca mulatta*. *Brain Res* 36: 229–249, 1972.

Penfield W, Erickson TC. *Epilepsy and Cerebral Localization; a Study of the Mechanism, Treatment and Prevention of Epileptic Seizures*. Springfield, IL: C. C. Thomas, 1941.

Pons TP, Wall JT, Garraghty PE, Cusick CG, Kaas JH. Consistent features of the representation of the hand in area 3b of macaque monkeys. *Somatosens Res* 4: 309–331, 1987.

Rabinowitz NC, Willmore BD, Schnupp JW, King AJ. Contrast gain control in auditory cortex. *Neuron* 70: 1178–1191, 2011.

Raichle ME, MacLeod AM, Snyder AZ, Powers WJ, Gusnard DA, Shulman GL. A default mode of brain function. *Proc Natl Acad Sci USA* 98: 676–682, 2001.

Ress D, Backus BT, Heeger DJ. Activity in primary visual cortex predicts performance in a visual detection task. *Nat Neurosci* 3: 940–945, 2000.

Reynolds JH, Heeger DJ. The normalization model of attention. *Neuron* 61: 168–185, 2009.

Riesenhuber M, Poggio T. Hierarchical models of object recognition in cortex. *Nat Neurosci* 2: 1019–1025, 1999.

Riesenhuber M, Poggio T. Neural mechanisms of object recognition. *Curr Opin Neurobiol* 12: 162–168, 2002.

Ringach DL. Population coding under normalization. *Vision Res* 50: 2223–2232, 2010.

Ruben J, Krause T, Taskin B, Blankenburg F, Moosmann M, Villringer A. Sub-area-specific suppressive interaction in the BOLD responses to simultaneous finger stimulation in human primary somatosensory cortex: evidence for increasing rostral-to-caudal convergence. *Cereb Cortex* 16: 819–826, 2006.

Sanchez-Panchuelo RM, Besle J, Beckett A, Bowtell R, Schluppeck D, Francis S. Within-digit functional parcellation of Brodmann areas of the human primary somatosensory cortex using functional magnetic resonance imaging at 7 tesla. *J Neurosci* 32: 15815–15822, 2012.

Sanchez-Panchuelo RM, Francis S, Bowtell R, Schluppeck D. Mapping human somatosensory cortex in individual subjects with 7T functional MRI. *J Neurophysiol* 103: 2544–2556, 2010.

Saproo S, Serences JT. Attention improves transfer of motion information between V1 and MT. *J Neurosci* 34: 3586–3596, 2014.

Sceniak MP, Hawken MJ, Shapley R. Visual spatial characterization of macaque V1 neurons. *J Neurophysiol* 85: 1873–1887, 2001.

Sceniak MP, Ringach DL, Hawken MJ, Shapley R. Contrast's effect on spatial summation by macaque V1 neurons. *Nat Neurosci* 2: 733–739, 1999.

Schwartz O, Simoncelli EP. Natural signal statistics and sensory gain control. *Nat Neurosci* 4: 819–825, 2001.

Schweisfurth MA, Schweizer R, Frahm J. Functional MRI indicates consistent intra-digit topographic maps in the little but not the index finger within the human primary somatosensory cortex. *Neuroimage* 56: 2138–2143, 2011.

Schweizer R, Voit D, Frahm J. Finger representations in human primary somatosensory cortex as revealed by high-resolution functional MRI of tactile stimulation. *Neuroimage* 42: 28–35, 2008.

Scolari M, Byers A, Serences JT. Optimal deployment of attentional gain during fine discriminations. *J Neurosci* 32: 7723–7733, 2012.

Serences JT, Saproo S. Computational advances towards linking BOLD and behavior. *Neuropsychologia* 50: 435–446, 2012.

Shmuel A, Augath M, Oeltermann A, Logothetis NK. Negative functional MRI response correlates with decreases in neuronal activity in monkey visual area V1. *Nat Neurosci* 9: 569–577, 2006.

Shmuel A, Leopold DA. Neuronal correlates of spontaneous fluctuations in fMRI signals in monkey visual cortex: implications for functional connectivity at rest. *Hum Brain Mapp* 29: 751–761, 2008.

Shmuel A, Yacoub E, Pfeuffer J, Van de Moortele PF, Adriany G, Hu X, Ugurbil K. Sustained negative BOLD, blood flow and oxygen consumption response and its coupling to the positive response in the human brain. *Neuron* 36: 1195–1210, 2002.

Simoncelli EP, Heeger DJ. A model of neuronal responses in visual area MT. *Vision Res* 38: 743–761, 1998.

Sinz FH, Bethge M. What is the limit of redundancy reduction with divisive normalization? *Neural Comput* 25: 2809–2814, 2013.

Smith AT, Williams AL, Singh KD. Negative BOLD in the visual cortex: evidence against blood stealing. *Hum Brain Mapp* 21: 213–220, 2004.

Smith MA, Bair W, Movshon JA. Dynamics of suppression in macaque primary visual cortex. *J Neurosci* 26: 4826–4834, 2006.

Stringer EA, Chen LM, Friedman RM, Gatenby C, Gore JC. Differentiation of somatosensory cortices by high-resolution fMRI at 7 T. *Neuroimage* 54: 1012–1020, 2011.

Sundberg KA, Mitchell JF, Reynolds JH. Spatial attention modulates center-surround interactions in macaque visual area v4. *Neuron* 61: 952–963, 2009.

Tommerdahl M, Favorov OV, Whitsel BL. Dynamic representations of the somatosensory cortex. *Neurosci Biobehav Rev* 34: 160–170, 2010.

Tootell RB, Hadjikhani N, Hall EK, Marrett S, Vanduffel W, Vaughan JT, Dale AM. The retinotopy of visual spatial attention. *Neuron* 21: 1409–1422, 1998.

Vokoun CR, Huang X, Jackson MB, Basso MA. Response normalization in the superficial layers of the superior colliculus as a possible mechanism for saccadic averaging. *J Neurosci* 34: 7976–7987, 2014.

Wade AR, Rowland J. Early suppressive mechanisms and the negative blood oxygenation level-dependent response in human visual cortex. *J Neurosci* 30: 5008–5019, 2010.

Wainwright MJ, Schwartz O, Simoncelli EP. Natural image statistics and divisive normalization. In: *Probabilistic Models of the Brain: Perception and Neural Function*, edited by Rao RP, Olshausen BA, Lewicki MS. Cambridge, MA: MIT Press, 2002, p. 203.

Woolsey TA, Rovainen CM, Cox SB, Henegar MH, Liang GE, Liu D, Moskalenko YE, Sui J, Wei L. Neuronal units linked to microvascular modules in cerebral cortex: response elements for imaging the brain. *Cereb Cortex* 6: 647–660, 1996.

Xing J, Heeger DJ. Center-surround interactions in foveal and peripheral vision. *Vision Res* 40: 3065–3072, 2000.

Xing J, Heeger DJ. Measurement and modeling of center-surround suppression and enhancement. *Vision Res* 41: 571–583, 2001.

Yacoub E, Shmuel A, Pfeuffer J, Van De Moortele PF, Adriany G, Andersen P, Vaughan JT, Merkle H, Ugurbil K, Hu X. Imaging brain function in humans at 7 Tesla. *Magn Reson Med* 45: 588–594, 2001.

Zenger-Landolt B, Heeger DJ. Response suppression in V1 agrees with psychophysics of surround masking. *J Neurosci* 23: 6884–6893, 2003.

Zoccolan D, Cox DD, DiCarlo JJ. Multiple object response normalization in monkey inferotemporal cortex. *J Neurosci* 25: 8150–8164, 2005.